

# Porous Al<sub>2</sub>O<sub>3</sub>/Al Metal Ceramics Prepared by the Oxidation of Aluminum Powder under Hydrothermal Conditions Followed by Thermal Dehydration:

## III. The Reactivity of Aluminum, the Reaction Mechanism of Its Oxidation with Water Vapor, and the Microtexture of Cermets

S. F. Tikhov, Yu. V. Potapova, V. A. Sadykov, V. B. Fenelonov, S. V. Tsybulya, A. N. Salanov, V. P. Ivanov, and V. N. Kolomiichuk

Boreskov Institute of Catalysis, Siberian Division, Russian Academy of Sciences, Novosibirsk, 630090 Russia

Received August 13, 2002

**Abstract**—The macrokinetics of aluminum oxidation under hydrothermal conditions at 150–250°C and water vapor pressures of ~0.5–4.5 MPa was studied. The apparent kinetic characteristics of the process were determined. The diffusion of water through the layer of a hydrated product was found to be a rate-limiting step. It was found that diffusion coefficients for various aluminum samples differed by almost two orders of magnitude; the main reaction steps were revealed. Changes in the texture of aluminum oxide in cermets in the course of the hydrothermal oxidation reaction were analyzed. This texture was found to depend on the ratio between the specific rate of the oxidation reaction and the rate of aging of the oxidation products under hydrothermal conditions.

### INTRODUCTION

Previously [1, 2], analytic expressions and empirical equations relating the pore volume and the specific surface area to the composition of Al<sub>2</sub>O<sub>3</sub>/Al composites, which depends on the conversion of aluminum at the step of hydrothermal oxidation, were derived. Therefore, an analysis of factors responsible for the conversion of aluminum in this reaction (temperature, water vapor pressure, and the specific reactivity of aluminum) is of crucial importance in the development of approaches to controlling the properties of cermets.

The studies of aluminum oxidation with water have a long history [3–8]. It was found that, at a temperature lower than the boiling point of water, the reaction rate passes through a maximum as aluminum undergoes oxidation [3, 5, 8]. The value and position of a maximum rate depend on the temperature of experiments and on the average particle size of aluminum powder. Thus, in coarsely dispersed powders, the time and conversion at which the rate reaches a maximum decreases with temperature; ~3–5% conversion at 60–70°C is reached in ~5–10 min [5, 7]. In submicron powders, a broad maximum of the rate lies in the range from ~8 to ~20% conversion [8]. Similar activation energies of 74 [3] and 54–113 kJ/mol [7] were published. Zhilinskii *et al.* [6] noted an increase in the activation energy from ~70 to ~108 kJ/mol with the dispersity of powders. The majority of authors believe that the occurrence of a maximum rate is due to the formation and growth of the reactive islands of a porous hydrated product in a pro-

TECTIVE film of aluminum oxide. At the point of a maximum, the specific rates of oxidation were comparable for all of the tested types of aluminum [3, 5, 8]; this should be observed when all the reactive islands merge and the apparent rate of reaction is proportional to the specific surface area of the metal. However, the specific rates of reaction were different in different powders under identical experimental conditions [6].

The conclusions about the nature of reaction products were even less consistent. Thus, according to data [5], an X-ray amorphous hydroxide was formed at the initial stage of the reaction; then, boehmite was formed, and bayerite was predominant after attaining a maximum rate. Lur'e *et al.* [3] did not specially study the nature of reaction products; however, they assumed a layer-by-layer arrangement of reaction products as the distance from the metal surface increased: oxide, boehmite, and bayerite. According to Anan'in *et al.* [7], the fraction of boehmite in the reaction products of highly dispersed aluminum is high, whereas the fraction of bayerite is low. No studies of the texture of oxides formed after the thermal decomposition of hydroxides were performed in the cited publications. Note that the kinetics was studied at temperatures lower than 100°C when the pressure of water vapor was approximately constant. Yakerson *et al.* [9] studied the effects of additives on the nature of hydrothermal oxidation products and the texture characteristics of the oxide obtained after thermal decomposition. They found that pseudo-boehmite and bayerite resulted from the interaction

**Table 1.** Diffusion coefficients for aluminum metal of different origins in the reaction of hydrothermal oxidation at 150°C and a vapor pressure of 0.5 MPa; characteristics of the parent aluminum samples

Sample	$D \times 10^{13}$ , cm <sup>2</sup> /s	SAXS data for parent samples*		Impurity concentrations**									
		$d$ , Å	$I$ , arb. u.	Na		K		Mg		Ca		Fe	
				$V$	$S$	$V$	$S$	$V$	$S$	$V$	$S$	$V$	$S$
PAVCh	167	103	105	0.01	8.0	0.02	9.3	0.07	4.0	0.002	4.6	0.01	15.0
PA-4	10	47	58	0.02	4.4	0.02	2.8	0.07	4.1	0.02	2.6	0.3	***
Foil	2	38	<10	0.01	13.1	0.03	4.7	0.01	2.2	0.04	2.4	0.2	2.7

\*  $d$  is the average size of nonuniformity regions;  $I$  is the SAXS signal intensity.

\*\*  $V$  is the bulk impurity concentration (according to chemical analysis data), wt %;  $S$  is the enrichment of a surface layer of ~20 Å with impurities (according to SIMS data), arb. u.

\*\*\* The concentration is lower than the mass-spectrometric detection limit.

with water, and the ratio between them depended on temperature and the amount of activator (In or Ga). In this case, the concentration of bayerite increased with temperature and the amount of activators. However, the kinetics of hydrothermal oxidation was not studied in [9].

In the only publication [7] where the oxidation process was studied at 120–230°C, kinetic measurements were performed using a simplified procedure: the conversion of aluminum after 2.5 h was determined at different temperatures. Two types of aluminum powders of different dispersity were studied. It was found that boehmite was the main product of hydrothermal oxidation under these conditions; however, the Al(OH)<sub>3</sub> trihydrate appeared as the temperature was decreased. The formation of product in the form of whiskers was mentioned, which was presumably explained by the occurrence of local centers of the preferred oxidation of aluminum (like dislocations). Additional studies of the resulting cermets after calcination in air revealed non-monotonic changes in the specific surface area depending on the temperature of hydrothermal treatment. However, the dependence of the rate of reaction on the pressure of water vapor was not determined in [7], and no rate equations, which make it possible to compare quantitatively the specific reactivity of aluminum of different genesis, were derived.

The previously obtained dependence of conversion on temperature and water vapor pressure was described by formal kinetics using the Roginskii–Schulz equation for a compressible sphere, which assumes the absence of detectable diffusion inhibition by a reaction product [10]. However, based on a more detailed analysis of kinetic curves, we subsequently concluded that the derived relations are closer to diffusion kinetics.

The aim of this work was to describe the data in terms of diffusion kinetics, to reveal a correlation between quantitative kinetic characteristics of the reac-

tion and the nature of the reaction products, to compare the specific reactivities of various types of aluminum metal, and to study the effect of the kinetics of hydrothermal oxidation of aluminum on the microtexture of the Al<sub>2</sub>O<sub>3</sub>/Al cermets obtained after calcination.

## EXPERIMENTAL

Aluminum powders of PA-4 and PAVCh grades and aluminum foil were used as starting reagents. The specific surface areas of the samples were 0.8, 1.2, and 0.0042 m<sup>2</sup>/g, respectively. Bulk impurity concentrations were determined by atomic absorption spectrophotometry (AAS-1) and atomic ionization spectrometry (Plasma Spectrovac). The chemical composition of reagent surfaces was determined by secondary ion mass spectrometry (SIMS) on an MS-7201 mass spectrometer (the energy of an Ar<sup>+</sup> beam was 4 keV at an etching rate of ~6 Å/min and a current density of 10–20 μA/cm<sup>2</sup>; the thickness of a test layer was ~20 Å). The powders were rubbed into a holder of high-purity indium. Table 1 summarizes the concentrations of impurities in the samples. The texture characteristics were determined on an ASAP 2400 Micromeritics instrument using the adsorption of nitrogen at 77 K.

The conditions of kinetic experiments were described in detail elsewhere [10, 11]. We varied temperature (150, 210, and 250°C), time (0.5–6.5 h), and water vapor pressure (500–4500 kPa). The temperature and water vapor pressure ranges were chosen because mechanically strong porous cermets are formed under these conditions [1, 7], and this was the main goal of this work. The final conversions of aluminum varied over the ranges ~0.1–4.0% for foil, ~7–25% for PA-4, and ~23–52% for PAVCh. The measurement error in aluminum conversion was ±10% of the determined value; it was mainly due to technical problems in the determination of sample weights in a press mold before

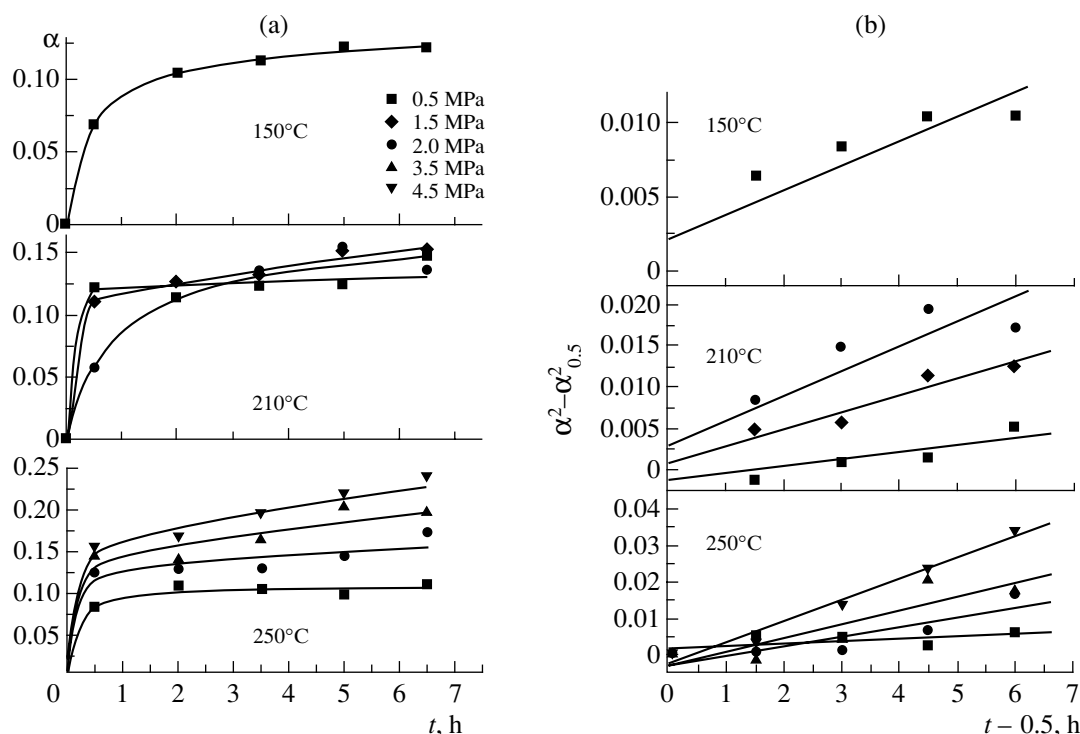


**Fig. 1.** (a) Aluminum conversion ( $\alpha$ ) as a function of the time of hydrothermal oxidation at different temperatures and water vapor pressures for the PA-4 powder. (b) The above function on the coordinates of a diffusion equation [13].

and after hydrothermal treatment and calcination. The vapor pressure was kept constant during each particular experiment. The procedures used for studying the samples by scanning electron microscopy, X-ray diffraction (XRD) analysis, small-angle X-ray scattering (SAXS), and adsorption techniques were described in detail previously [2, 12]. The SAXS signal intensity was determined in an angle region of  $7^\circ$  with reference to a primary X-ray beam in air.

## RESULTS AND DISCUSSION

### 1. General Analysis of Kinetic Curves

Figures 1a, 2a, and 2c demonstrate the time dependence of the conversion at different pressures of water vapor and temperatures for the PA-4 powder, the foil, and the PAVCh powder, respectively. As compared to previously published data [3], it can be seen that these plots are not *S*-shaped curves, which are characteristic of many topochemical reactions, with an induction period at the initial stage of reaction. In the oxidation of aluminum with water, this induction period is usually related to the slow degradation of a protective oxide film and the formation of a loose hydrated phase at the initial stage of reaction [4]. Under the conditions of our experiments, it is most likely that we skipped this stage, as well as the stage at which the rate increased to its maximum in the first half hour of reaction, before the analysis of the first experimental point. Moreover, with

the use of electron microscopy, we found that, even at the initial stages of reaction ( $t = 0.5$ – $2.0$  h), the surface of aluminum was fully coated with a porous product layer  $\sim 1$   $\mu\text{m}$  in thickness. This product was significantly different in morphology from the initial oxide films of powders [12] and aluminum foil [13]. Thus, in our case, the region in which the reagent is completely coated with a product layer of aluminum hydroxide is the most likely region of the occurrence of a topochemical reaction of aluminum oxidation with water.

An insignificant change in the specific surface area of the reagent in the tested region of aluminum conversions is another circumstance that is important for the subsequent kinetic analysis. This is approximately obeyed for aluminum foil because of extremely low aluminum conversions. This assumption was also supported by possible changes in the specific surface area of aluminum powders, as estimated taking into account their almost ideally spherical shape [12]. Indeed, the reaction rate is proportional to the mass of the remaining reagent, which depends on the conversion ( $\alpha$ ) and mass ( $m_0$ ) of the starting reagent. Moreover, the mass of the remaining reagent is proportional to its volume, which depends on the particle radius (in the monodisperse approximation):

$$w = km_0(1 - \alpha) \sim \rho_{\text{reag}} \frac{4}{3} \pi R^3, \quad (1)$$

where  $\rho_{\text{reag}}$  is the true density of the reagent and  $R$  is the particle radius. On the other hand, to a first approxima-

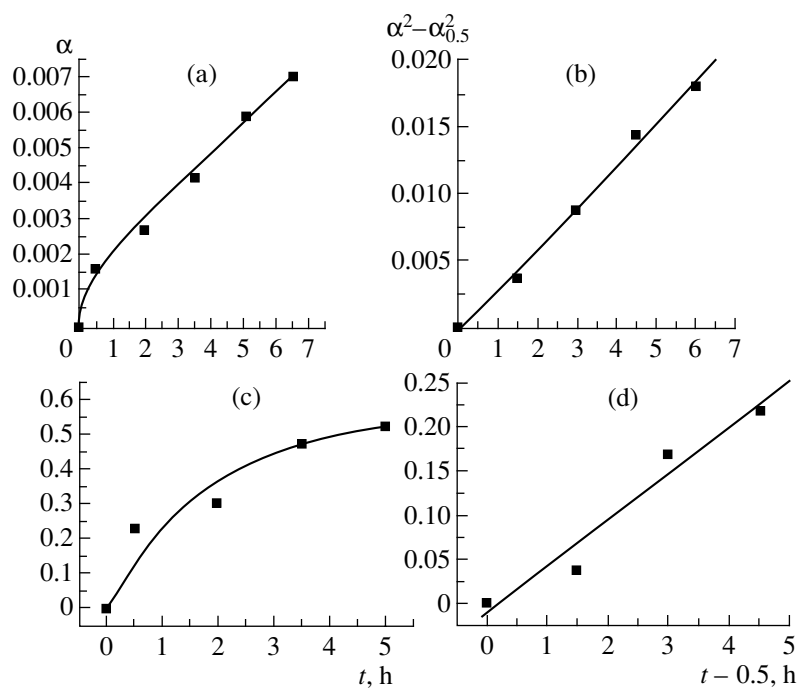


**Fig. 2.** Aluminum conversion ( $\alpha$ ) as a function of the time of hydrothermal oxidation at 150°C and a water vapor pressure of 0.5 MPa for (a) aluminum foil or (c) PAVCh; the above function on the coordinates of a diffusion equation [13] for (b) aluminum foil or (d) PAVCh.

tion, the specific surface area of spherical particles is proportional to the squared particle radius:

$$S \sim 4\pi R^2 \sim (1 - \alpha)^{2/3}. \quad (2)$$

With a maximum change in  $\alpha$  from 0 to 0.25 (see Fig. 1a), the reagent surface area is changed by a factor of 0.81, which lies within the limits of experimental error in kinetic measurements. The surface roughness of real particles usually results in a significant increase in the magnitude of the specific surface area of the reagent. However, it is most likely that the contribution of roughness decreases the dependence of the specific surface area on the conversion because a topochemical reaction hardly results in smoothing the reagent surface. Thus, to a first approximation, the specific surface area of aluminum can be considered constant over the entire ranges of tested aluminum conversions, temperatures, and water vapor pressures.

On this basis, we estimated the average apparent specific rates of reaction in the region  $t = 0.5\text{--}6.5$  h for PA-4 with the use of the simplified expression

$$w_{\text{sp}} = \frac{d\alpha}{dt} \frac{1}{S_{\text{sp}} M_{\text{Al}}} \times 10^{-4} \text{ mol Al cm}^{-2} \text{ h}^{-1}, \quad (3)$$

where  $M_{\text{Al}}$  is the molar weight of aluminum and  $S_{\text{sp}}$  is its specific surface area. At 150°C, the specific rate of reaction was found to equal  $\sim 0.04 \times 10^{-6} \text{ mol Al cm}^{-2} \text{ h}^{-1}$ . We compared this value with the specific rate of reaction at a maximum point ( $w_{\text{sp}} \approx 5 \times 10^{-6} \text{ mol Al cm}^{-2} \text{ h}^{-1}$ ), which was obtained for an ASD-4 powder with charac-

teristics similar to those of the PA-4 powder used in this study (by the extrapolation of data obtained below the boiling point of water to  $T = 150^\circ\text{C}$  using the equation  $w_{\text{sp}} = 10^{22} \exp(-17500/RT)$  [3]). This comparison showed that the extrapolated rate of reaction is higher than the experimental value by two orders of magnitude. Usually, the majority of authors cited comparable reaction rates (at least at temperatures lower than 100°C) for a maximum point when the reaction zone is proportional to the specific surface area. The difference between the reaction rate taken from [3], which was extrapolated to high temperatures, and the experimental value obtained in this work cannot be explained only by the difference in the specific reactivities of different aluminum powders or by the difference in water vapor pressures. Most likely, this may be due to a change in the reaction mechanism (the shape of a kinetic curve) at high temperatures, as compared with temperatures below 100°C. Consequently, the equation derived by Lur'e *et al.* [3] is inapplicable to our conditions, and the reaction mechanism is significantly different. Note that at the initial portion ( $t = 0\text{--}0.5$  h) the reaction rate for the PA-4 powder was much higher ( $\sim 1 \times 10^{-6} \text{ mol Al cm}^{-2} \text{ g}^{-1}$ ). Thus, the experimental rate of aluminum oxidation at the initial portion was much closer to the maximum point of the rate of a topochemical reaction, which could be assumed on the extrapolation of published data to be 150°C.

The results allowed us to conclude that under the conditions of our experiments the majority of experi-

mental points occurred in a region after the maximum point, when the reaction rate of aluminum oxidation decreased with time.

## 2. Diffusion Coefficients for Different Aluminum Samples

It is well known that a decrease in the rate of a topochemical reaction after reaching a maximum is usually due to an increase in the thickness of a product layer, which inhibits the reaction (the reaction rate is proportional to the amount of a converted substance) [16]. To estimate the coefficients of diffusion through a product layer, we used the well-known parabolic equation [16, 17]

$$\alpha^2 - \alpha_{0.5}^2 = k'(t - 0.5), \quad (4)$$

where  $\alpha$  and  $\alpha_{0.5}$  are the conversions of aluminum at times  $t$  and 0.5 h, respectively. The modified parabolic equation was used because at the initial portion (0–0.5 h) the state of the catalyst surface (the mechanism of a heterogeneous reaction) is uncertain; this uncertainty resulted in a significant change in the function  $\alpha(t)$ , as compared with the subsequent points (Figs. 1, 2).

An analysis of kinetic curves linearized on the coordinates of a parabolic equation (Figs. 1b, 2b, 2d) demonstrated that the experimental points for the foil, PAVCh, and, partially, PA-4 adequately lay along a straight line. In the PA-4 powder, some of the points at 150 and 210°C significantly deviated from the linearized curves. The standard deviation of  $k'$ , which is determined by the slopes of these kinetic curves (Fig. 1b), may be up to 30% due to the deviation of the specific surface area of the reagent from the initial value. The effect of diffusion processes within a grain of the porous cermet formed may be another factor that can deviate linearized curves from the origin of the coordinates and increase the scatter of experimental points. Thus, the linearized curves for aluminum foil, where this factor is insignificant, clearly passed through the origin (Figs. 2a, 2b). The change of the porous structure of the composite with time complicates the quantitative description of the diffusion effect within a grain [1]. However, these factors did not appear in the PAVCh powder. It is likely that the transition to the diffusion region was incomplete for PA-4. At the same time, as a first approximation, it is believed that the reagent diffusion through a hydrated product layer was predominant in the reaction of aluminum with water under our conditions.

Note that these data were adequately linearized previously [10] on the coordinates of the Roginskii–Schulz equation, which is based on the assumption that the apparent rate of reaction is proportional to a change in the reagent surface area. In this case, a paradoxical situation occurred when the same experimental data are described by different rate equations within the accuracy of the experiment. The models should be distin-

guished from an analysis of specific properties of the test system [16]. Indeed, a subsequent detailed analysis of the kinetic curves revealed that in our case a change in the derivative of conversion with respect to time was much greater (Fig. 1a) than the possible change in the specific surface area of the reagent.

The diffusion coefficients were estimated from the values of  $k'$  based on the assumption that the specific surface area of the reagent is approximately constant using the equation proposed by Rozovskii [16]. Moreover, because this equation was derived on the approximation of a one-dimensional problem, it was reasonable to change to the bulk reagent (water vapor) concentrations. This allowed us to obtain the following expression for the diffusion coefficient:

$$D = \frac{M_{\text{AlOOH}} m_{0,\text{Al}}^2 k'}{2 C_0 \rho_{\text{AlOOH}} S_{\text{Al}} M_{\text{Al}}^2} = \frac{M_{\text{AlOOH}} k'}{2 C_v \rho_{\text{AlOOH}} S_{\text{sp}}^2 M_{\text{Al}}^2}, \quad (5)$$

where  $C_v = \frac{C_0}{S_{\text{Al}}} = \frac{C_0}{S_{\text{sp}} m_0}$ ,  $D$  is the diffusion coefficient (cm<sup>2</sup>/s),  $\rho_{\text{AlOOH}}$  is the density of aluminum hydroxide produced from aluminum,  $M$  is the molar weight of aluminum and the hydroxide,  $C_0$  is the reagent concentration at the outer surface of the product in a one-dimensional approximation (mol/cm),  $S_{\text{Al}}$  is the geometric surface of the reagent, and  $S_{\text{sp}}$  is the specific surface area of the reagent (m<sup>2</sup>/g).

In Eq. (5), the density of aluminum hydroxide was estimated from data on the density and composition of AlOOH/Al cermets. At 150°C, it was 2.4, 2.7, and 2.4 g/cm<sup>3</sup> for PA-4, PAVCh, and foil, respectively. For PA-4, the density of aluminum hydroxide at 210 and 250°C was taken to be equal to 3.0 and 3.4 g/cm<sup>3</sup>, respectively. These values are somewhat different from the tabulated data in [18]. The reasons for this phenomenon were discussed previously [2]. The concentration of water vapor was calculated using the ideal gas equation

$$C_v = \frac{n}{V} = \frac{P_{\text{H}_2\text{O}}^m}{RT}, \quad (6)$$

where  $P_{\text{H}_2\text{O}}$  is the pressure of water vapor in an autoclave at temperature  $T$ . The dependence of the constant of a hyperbolic equation ( $k'$ ) on the pressure of water vapor was preestimated (the apparent order of reaction ( $m$ ) (Fig. 3a) was 0.9). The sufficiently strong dependence on the pressure of water vapor allowed us to conclude that, in accordance with [6], the diffusion of water rather than aluminum cations is the rate-limiting step of the process.

Note that, according to the Kelvin equation, which determines the minimum size of pores in which water vapor can condense [14], the surface of cermets was completely covered with water in the course of hydrothermal oxidation at equilibrium pressures and all tem-

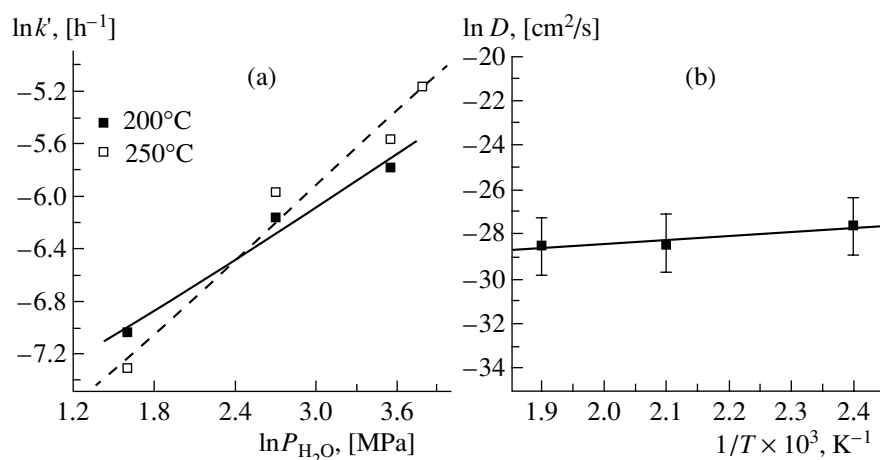


**Fig. 3.** (a) Determination of the reaction order with respect to water for the oxidation of PA-4 from data shown in Fig. 1. (b) The temperature dependence of diffusion coefficients on the Arrhenius coordinates for PA-4.

peratures. At lower vapor pressures, the radius of pores in which water condensation is possible decreased from 90 to 3 Å as the pressure was decreased from 1.5 to 0.5 MPa at 210°C or from 15 to ~1 Å as the pressure was decreased from 3.5 to 0.5 MPa at 250°C, as calculated using the Laplace–Kelvin equation. Thus, in the majority of kinetic experiments under conditions of hydrothermal oxidation, water can condense in only micropores, which usually occur in the interlayer space of hydroxides, and the amount of water decreases with temperature. However, as distinct from the reaction of iron oxidation with water [15], no considerable changes were observed in the dependence of the conversion on the time of hydrothermal oxidation under conditions of an equilibrium vapor pressure, nor in the dependence obtained at lower pressures (Fig. 1a). It is likely that, under conditions when the diffusion of water vapor is a rate-limiting step, the concentration of water at the surface of a solid reagent (aluminum) is close to zero, and the apparent rate of reaction depends on both water concentration at the outer surface of a hydroxo compound and the diffusion permeability of this compound.

Table 1 indicates that the diffusion coefficients obtained at 150°C in different samples differ by almost two orders of magnitude. Because the reaction is limited by diffusion, the diffusion coefficient practically characterizes the specific reactivity of aluminum. Note that considerable differences in the diffusion coefficients of water at temperatures lower than 100°C were also observed previously in different aluminum powders. This was related to differences in the dispersity of powders and, as a consequence, in the degrees of crystallinity of protective oxide layers [6]. However, in our case, the average particle sizes of both of the powders were similar and equal to 20–25 μm, as evaluated using the Coulter method [12].

Note that the X-ray diffraction patterns of aluminum foil, which exhibits the lowest reactivity, contain prac-

tically no peaks with (111) indices, as distinct from aluminum powder samples. This difference was also retained after partial oxidation of aluminum. This fact is indicative of a preferential orientation of crystallites with respect to the surface of foil, probably due to the effect of rolling in the course of its manufacture. However, this phenomenon cannot explain the considerable difference between the diffusion coefficients of the two powdered samples.

We also determined bulk and surface impurity concentrations in the test samples of aluminum. We found that the bulk concentrations of alkaline-earth metal impurities in all of the samples were comparable (Table 1). The enrichment of an aluminum surface with impurities, as compared with the bulk, is typical (Table 1). The surface concentrations of alkaline-earth metals in the PAVCh and foil samples were several times higher than that in PA-4. The foil and PA-4 differ from PAVCh in that they have considerably higher bulk iron contents. Generally, no correlation between the diffusion coefficients and impurity concentrations was observed.

The SAXS data, which were used for the analysis of the texture characteristics of oxide films that cover aluminum, allowed us to conclude that changes in the concentrations of regions with a nonuniform electron density and in diffusion coefficients exhibit similar patterns (greater SAXS signal intensities correspond to greater values of  $D$ ) (Table 1). Indeed, previously [2], it was found that SAXS data characterize both qualitatively (by the distribution of these regions) and quantitatively (by the intensity of signals) oxide rather than metal components of cermets. The SAXS signal as an integrated characteristic depends on the sizes of both primary particles and oxide pores. Taking into account that in this case SAXS characterizes oxide films, which cover the surface (partially hydrated because of contact with humid air) of starting samples, it is believed that the diffusion coefficients essentially depend on the tex-

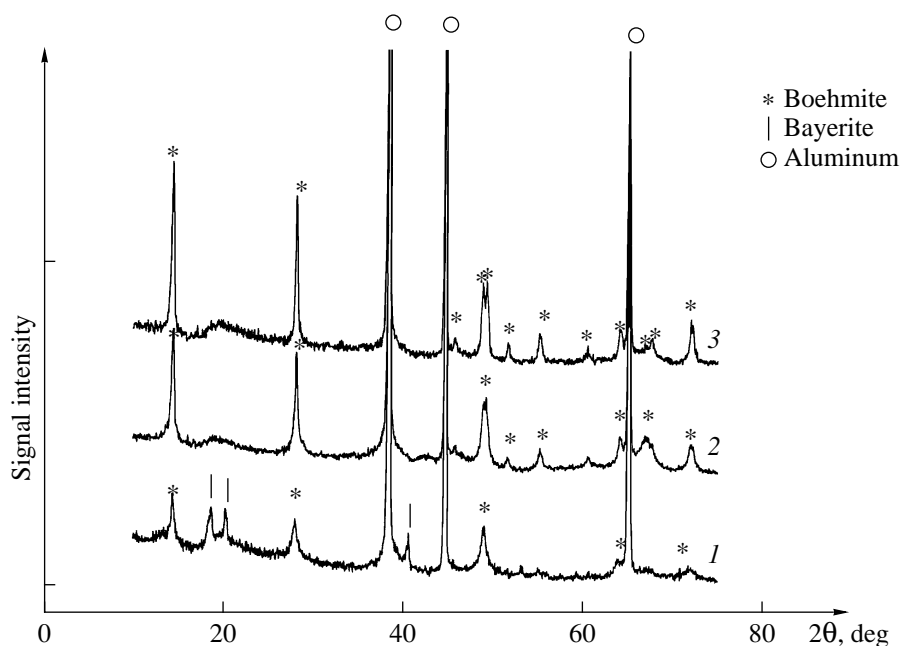


**Fig. 4.** X-ray diffraction patterns of aluminum powder samples after hydrothermal oxidation (HTO) and drying at 120°C: (1) PAVCh,  $T_{\text{HTO}} = 150^\circ\text{C}$ ,  $t_{\text{HTO}} = 0.5$  h; (2) PAVCh,  $T_{\text{HTO}} = 150^\circ\text{C}$ ,  $t_{\text{HTO}} = 5.0$  h; (3) PA-4,  $T_{\text{HTO}} = 250^\circ\text{C}$ ,  $t_{\text{HTO}} = 6.5$  h.

ture characteristics of these films, primarily, on pore size and volume (“free” area of the film). The relation of the oxide film texture of the parent metal to the texture of the hydrated oxidation product can be explained by a memory effect. In this case, the structure and texture characteristics of aluminum hydroxides depend on the structural characteristics of particles formed at the early stages of aluminum oxidation; these particles were retained even after long-term aging. These oriented growth processes, in which the particle structure and texture of aging products essentially depend on the structure and texture of parent reagent particles, are well known [19]. It is likely that stronger correlations can be obtained from a comparison of SAXS intensities with the initial rates of oxidation or from a study of hydrothermal oxidation products (aluminum hydroxides), which was beyond the scope of this work. The effect of product properties on kinetic characteristics was also supported by the apparent activation energy, which was formally found to be negative, about  $-16$  kJ/mol, which is close to zero (Fig. 3b). However, the negative temperature dependence of diffusion coefficients can also be explained by product consolidation and, as a consequence, a decrease in the diffusion permeability with temperature.

### 3. The Nature of Products and the Sequence of Hydrothermal Oxidation Reaction Steps

The X-ray diffraction data (Fig. 4) indicate that bayerite was formed at the initial stages of reaction in the hydrothermal oxidation of the highly reactive PAVCh powder. At the onset of reaction, bayerite disappeared

after 5 h; it transformed into boehmite. In the less reactive PA-4 powder, boehmite as the product of hydrothermal oxidation was observed at all the contact times over the entire range of tested temperatures (Fig. 4). Thus, under the conditions of our hydrothermal oxidation experiments, boehmite, which is more stable, was formed from bayerite. Such a reaction sequence of hydroxides on aging under hydrothermal conditions was also observed previously [19]. Under our conditions, it is likely that the ratio between these two species depends on the ration between the rates of bayerite formation and rearrangement into boehmite. The higher the specific reactivity of aluminum, the higher the above ratio. An amorphous hydroxide is the most probable primary porous product of oxidation. A halo at  $20^\circ$  in the X-ray diffraction patterns (Fig. 4) supported the occurrence of the above hydroxide in all of the samples of oxidation products. In this case, it is most likely that the formation of bayerite results from the aging of a loose amorphous product; this behavior is typical of hydroxide aging processes [19]. Note that the aging of hydroxides should become slower with decreasing pressure of water vapor. Indeed, a comparison of Figs. 5a and 6a–6c clearly indicates that the size and the degree of crystallinity of product particle agglomerates decrease with decreasing pressure of water vapor in an autoclave.

Thus, the following main steps responsible for the chemistry of hydrothermal oxidation can be recognized:



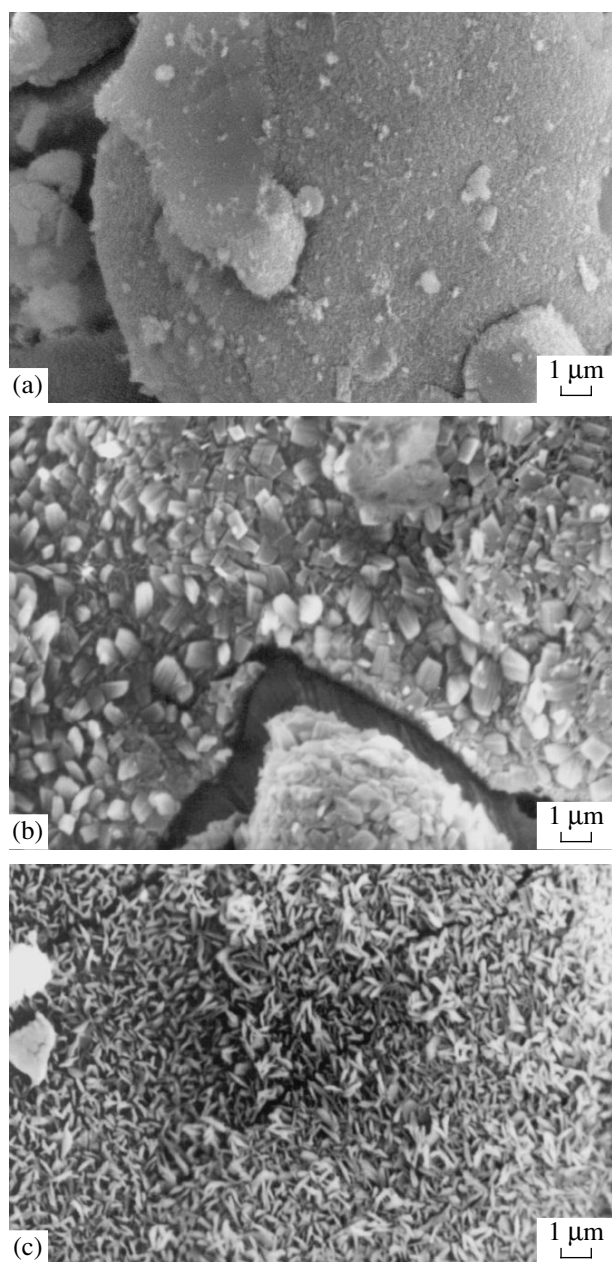
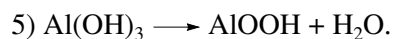
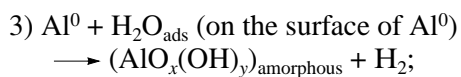
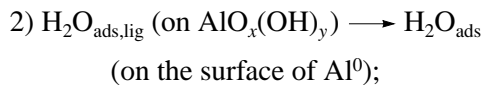


**Fig. 5.** Electron micrographs of  $\text{Al}_2\text{O}_3/\text{Al}$  composites prepared from (a) PAVCh, (b) PA-4, and (c) aluminum foil by hydrothermal oxidation at  $250^\circ\text{C}$  for 0.5 h followed by calcination in air.



Most likely, these steps are not elementary. The adsorption of water (condensation) in the pores of a hydroxo

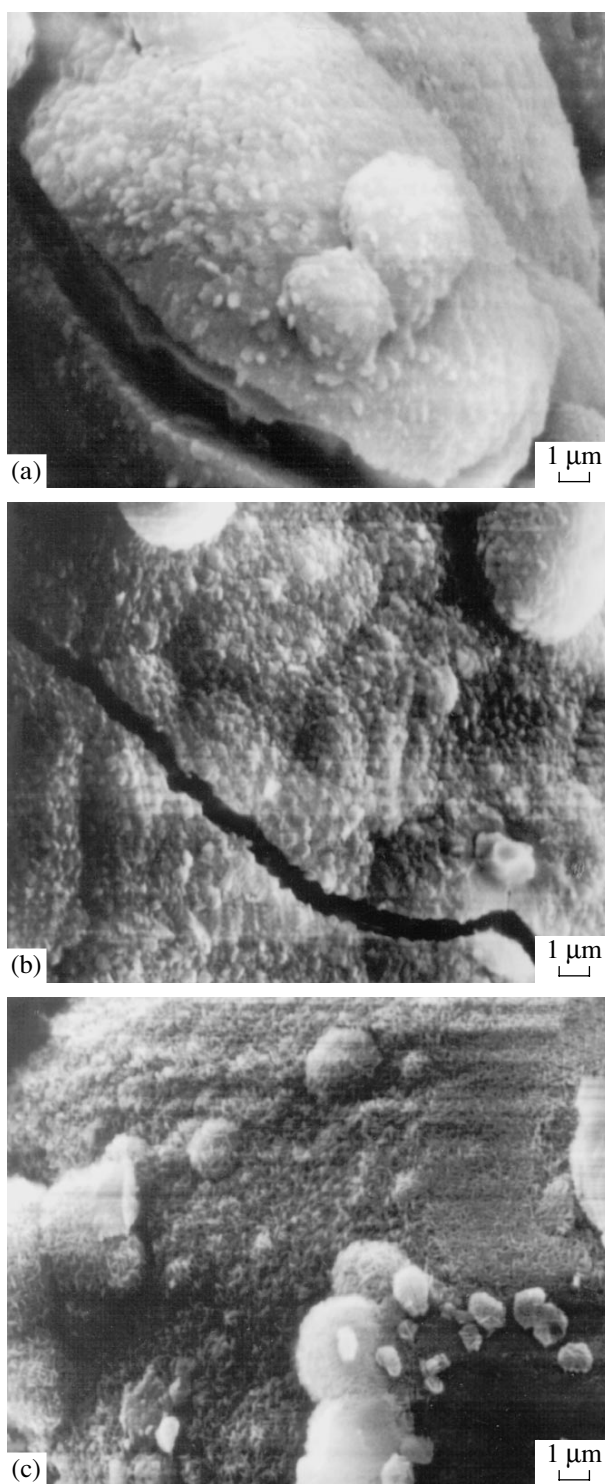


**Fig. 6.** Electron micrographs of  $\text{Al}_2\text{O}_3/\text{Al}$  composites prepared from PA-4 by hydrothermal oxidation at  $250^\circ\text{C}$  and the following vapor pressures, MPa: (a) 3.5 ( $t_{\text{HTO}} = 0.5$  h), (b) 2.0 ( $t_{\text{HTO}} = 3.5$  h), and (c) 0.5 ( $t_{\text{HTO}} = 6.5$  h).

compound of aluminum takes place at step (1). At step (2), water diffusion becomes limiting after the formation of a continuous product layer. Step (3) characterizes the

oxidation of aluminum with water and is very fast. Steps (4) and (5) characterize the evolution of reaction products. So-called polynuclear hydroxo complexes [19], whose structure can depend on external conditions, impurity concentrations, etc., can be the loose products that form amorphous aluminum hydroxide. A more detailed description of the hydrothermal oxidation reaction requires a much greater body of kinetic information.

#### 4. Effect of Product Aging under Hydrothermal Conditions on the Microtexture of Aluminum Oxide in Cermet after Calcination

Under conditions of hydrothermal oxidation, the resulting hydroxide particles undergo aging simultaneously with the chemical processes described above. This affects both the texture of these particles and the final texture of aluminum oxide after calcination [2]. Indeed, the specific surface area of aluminum oxide in cermets decreased (at the stage of hydrothermal oxidation) from  $\sim 320$  to  $\sim 200$   $\text{m}^2/\text{g}$  for PAVCh, from  $\sim 250$  to  $\sim 150$   $\text{m}^2/\text{g}$  for PA-4, and from  $\sim 350$  to  $\sim 70$   $\text{m}^2/\text{g}$  for the foil as the conversion increased (see Fig. 7 and Fig. 1 in [2]). Anan'in *et al.* [7] observed a similar decrease in the specific surface area of aluminum oxide in  $\text{Al}_2\text{O}_3/\text{Al}$  cermets as the conversion of aluminum increased (upon the corresponding quantitative treatment of experimental data). In this case, two tendencies can be recognized in changes in the specific surface area of an oxide phase:

(a) A decrease in the specific surface area with the degree of reaction to an approximately constant level (Fig. 7, Table 2).

(b) A decrease in the "constant level" of the specific surface area with decreasing reactivity of aluminum (Figs. 7 and 1 in [2]).

Taking into account a correlation between the specific surface areas of hydroxides and oxides, we can conclude that this phenomenon is analogous to the aging of products deposited under hydrothermal conditions, which was described in considerable detail for the hydroxo compounds of aluminum [19, 20]. This conclusion was also supported by the fact that boehmite, which is most stable under these conditions, was the final product of both hydrothermal oxidation at  $150\text{--}250^\circ\text{C}$  and aging at these temperatures [19, 20].

A correlation between the diffusion coefficients and the microtexture of aluminum oxide was found in a texture study based on a detailed analysis of nitrogen adsorption-desorption isotherms at 77 K for cermets prepared from PAVCh in comparison with PA-4 [2]. It was impossible to study cermets prepared from the foil because of the low oxide content.

Thus, we found that the shape of a hysteresis loop in the PAVCh cermet formed at the early stages of hydrothermal oxidation was closer to the H3 type according to the IUPAC classification [14]. However, it

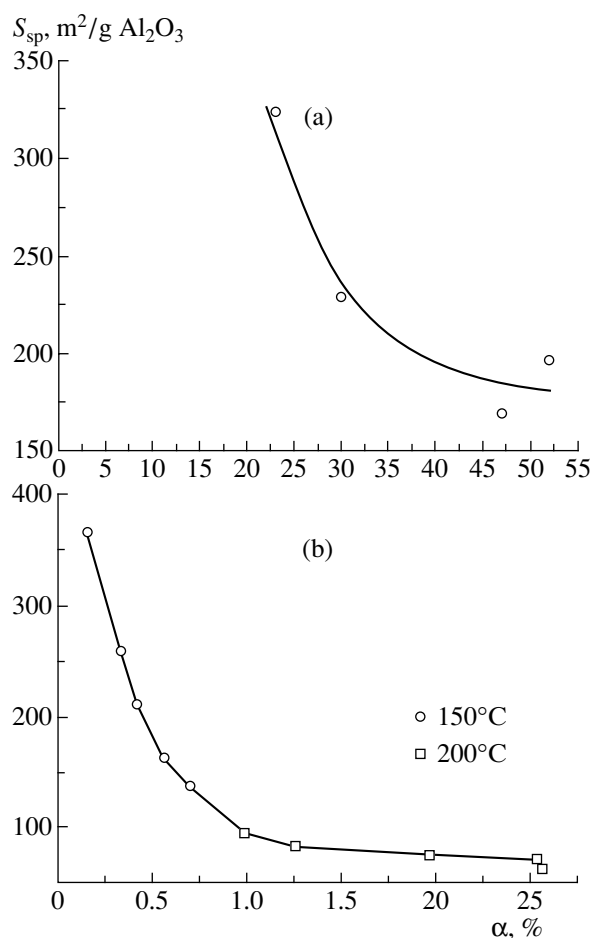


**Fig. 7.** Specific surface area ( $S_{sp}$ ) of aluminum oxide in  $\text{Al}_2\text{O}_3/\text{Al}$  cermets formed after hydrothermal oxidation and calcination as a function of aluminum conversion ( $\alpha$ ) in the hydrothermal oxidation of (a) PAVCh and (b) foil samples.

approached the H2 type, which is characteristic of PA-4 (Fig. 8), as the degree of reaction increased. Figure 9 shows the adsorption isotherms for cermets prepared from PAVCh as comparative plots [21, 22]. A standard  $\text{N}_2$  adsorption isotherm was used as a reference standard (the axis of abscissas) for constructing the comparative plots. This standard adsorption isotherm was obtained by averaging over several nonporous samples of different chemical nature [21]. This isotherm coincided with the standard adsorption isotherm proposed by Gregg and Sing [14] in the region of relative pressures  $P/P_0 < 0.7$ . The experimental adsorption deviated from linearity in the region of minimum coverages because of the effect of the nature of the surface, which has no effect on specific surface areas measured from the slopes of the linear plots [22]. Dotted lines in these plots demonstrate two linear portions: first, in the region of comparatively low  $P/P_0$  and, second, in the region of high  $P/P_0$  for the desorption branch of the isotherm. The first linear portion in Figs. 9a and 9b is extrapolated to the origin of the coordinates; this fact is

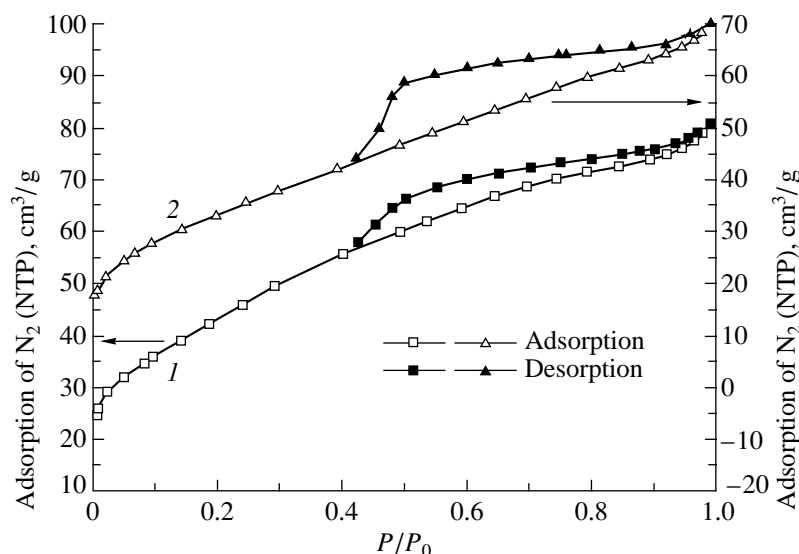


**Fig. 8.** Adsorption–desorption isotherms of nitrogen at 77 K for  $\text{Al}_2\text{O}_3/\text{Al}$  composites prepared from PAVCh;  $t_{\text{HTO}} = (1)$  0.5 or (2) 5.0 h. The gas volume was converted to normal temperature and pressure (NTP).

indicative of the absence of micropores. (Strictly speaking, the extrapolated comparative plot in Fig. 9 intersects the axis of abscissas at the point of  $\sim 0.0005$  due to the contribution of ultramicropores, whose volume is extremely small.) Note that, previously, the linearization of this portion for cermets prepared from PA-4 was somewhat different; however, the contribution of micropores to the total pore volume was insignificant [2].

Table 2 summarizes the results of an analysis of adsorption isotherms for cermets prepared from PAVCh (Fig. 8). It can be seen in Table 2 that the outer surface of aggregates in the cermets prepared from the PAVCh powder decreased with the time of hydrothermal oxidation. This outer surface was found from the slope of the second linear portion of the isotherm, which corre-

sponds to the remainder surface after the filling of mesopores in aggregates ( $S_{\text{outer}}$ ). The mesopore volume ( $V_s$ ), which was determined by the extrapolation of the second linear portion to the axis of ordinates, also decreased. This fact suggests that aging processes occur simultaneously with the chemical process of aluminum oxidation and affect the texture properties of the product: an increase in the size of primary particles, a change in the character of their packing, and an increase in the size of aggregates formed by these particles.

The specific pore volumes ( $V_a$ ) and the specific surface areas of aluminum oxides in cermets ( $S_{\text{Al}_2\text{O}_3}$ ) are also given in Table 2. These data were obtained from

**Table 2.** Microtexture characteristics of the  $\text{Al}_2\text{O}_3/\text{Al}$  composites prepared from the PAVCh powder according to nitrogen adsorption–desorption isotherms

Sample	Conditions of hydrothermal oxidation	$\text{Al}_2\text{O}_3$ content, wt %	Pore volume of the composite $\text{cm}^3/\text{g}$		Specific surface area of the composite, $\text{m}^2/\text{g}$			Texture characteristics of $\text{Al}_2\text{O}_3$		
			$V_s$	$V_a$	$S_{\text{BET}}$	$S_{\Sigma}$	$S_{\text{outer}}$	$V_{a, \text{Al}_2\text{O}_3}$ , $\text{cm}^3/\text{g}$	$S_{\Sigma, \text{Al}_2\text{O}_3}$ , $\text{m}^2/\text{g}$	$S_{\text{BET}, \text{Al}_2\text{O}_3}$ , $\text{m}^2/\text{g}$
PAVCh (0.5 h)	150°C, 0.5 h, 0.5 MPa	38.7	0.094	0.094	139	129	14.8	0.243	333	359
PAVCh (5.0 h)	150°C, 5.0 h, 0.5 MPa	58.4	0.090	0.090	121	135	11.6	0.154	231	205

Note: The pore volume was estimated using the balance equation  $V_s = V_{\text{Al}}(1 - y) + V_a y$ , where  $y$  is the oxide fraction in the cermet. The specific surface area was estimated using the balance equation  $S_{\Sigma} = S_{\text{Al}}(1 - y) + S_{\text{Al}_2\text{O}_3} y$ .  $V_a$  is the specific volume of micropores and mesopores within aggregates.  $V_s$  is the mesopore volume.  $S_{\Sigma}$  is the total specific surface area of composites found by a comparative analysis of adsorption isotherms.  $S_{\text{outer}}$  is the outer surface area of aggregates.

the composition of samples on the assumption that both the pore volume and the specific surface area of the oxide component are much greater than those of powdered aluminum, as was found previously [2]. A comparison between the texture properties of aluminum oxides obtained from PAVCh (Table 2) and PA-4 [2] suggests that, given the same synthesis time, both the total specific surface area and the pore volume referred to the weight of the oxide were greater in Al<sub>2</sub>O<sub>3</sub> from PAVCh. This can easily be explained by the much higher rate of oxidation of the PAVCh aluminum. Under comparable conditions of aging and oxidation of PAVCh under equal conditions, the fraction of smaller product particles is much higher; this results in the observed texture differences. Another difference between hydrothermal oxidation products from PAVCh and PA-4 is as follows: the former exhibited a much greater (by a factor of 4 to 5) outer surface (and hence a smaller size) of aggregates of primary particles. Consequently, under comparable external conditions of hydrothermal oxidation, higher specific reactivity resulted in the formation of smaller particles, which formed smaller aggregates. This can clearly be seen by comparing the scanning electron micrographs of PAVCh and PA-4 (Fig. 5). It is likely that aging processes rather than nonuniformities in the growth of product particles at individual local points, as assumed by Anan'in *et al.* [7], are primarily responsible for the formation of elongated well-crystallized aggregates. The behavior of particles formed in the hydrothermal oxidation of the foil (Fig. 5c) is inconsistent with the above pattern. This can be explained by the considerable change in the conditions of water vapor condensation on the surface of a plate as compared with pores between the particles of powdered aluminum; this change can affect the conditions of hydroxide aging.

Turning back to the reasons for differences in diffusion coefficients, we believe that the texture characteristics of the aluminum oxide formed (and hence the hydroxide) can significantly affect the diffusion of water through the product layer. As noted above, a denser product more strongly inhibits the oxidation reaction. Indeed, the average specific volume of micropores and mesopores in aluminum oxide from PAVCh (Table 2) was greater by 20–30% than that for PA-4 (Table 2 in [2]).

Thus, we studied the macrokinetics of the hydrothermal oxidation of aluminum at elevated temperatures, found the apparent kinetic parameters of the process, and compared the diffusion coefficients of various aluminum metal samples. We made assumptions about the factors responsible for differences in the diffusion coefficients and about the nature of the main reaction steps. We analyzed the relationship between the microtexture and the specific reactivity of the resulting cermet.

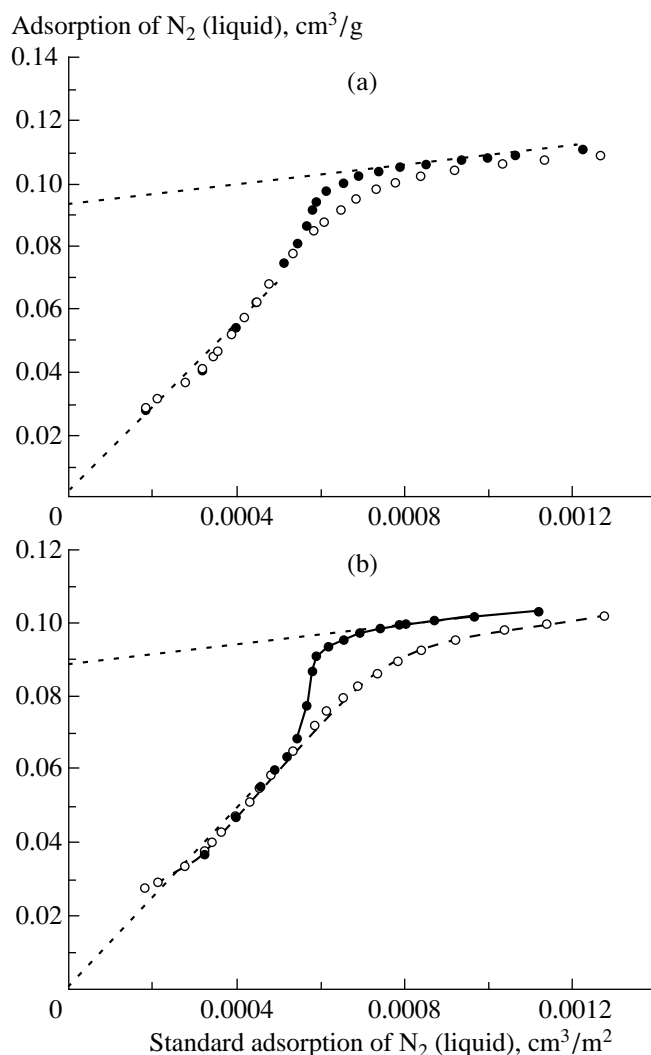


**Fig. 9.** Comparative plots of the adsorption–desorption isotherms of nitrogen at 77 K for composites prepared from PAVCh (Fig. 8);  $t_{\text{HTO}}$  = (a) 0.5 or (b) 5.0 h. Open and closed circles correspond to adsorption and desorption, respectively. The gas volume was converted to the volume of liquid condensed at 77 K. Data for the standard N<sub>2</sub> adsorption isotherm (see the text) are plotted on the abscissa.

#### ACKNOWLEDGMENTS

This work was supported by the Russian Foundation for Basic Research (project no. 99-03-32853). We are grateful to A.Ya. Rozovskii for helpful discussions of the results. Yu.V. Potapova acknowledges the support of INTAS (grant no. YFS-00-199).

#### REFERENCES

1. Tikhov, S.F., Felonov, V.B., Sadykov, V.A., Potapova, Yu.V., and Salanov, A.N., *Kinet. Katal.*, 2000, vol. 41, no. 6, p. 907.
2. Tikhov, S.F., Zaikovskii, V.I., Felonov, V.B., Potapova, Yu.V., Kolomiichuk, V.N., and Sadykov, V.A., *Kinet. Katal.*, 2000, vol. 41, no. 6, p. 916.

3. Lur'e, B.A., Chernyshev, A.N., Perova, N.N., and Svetlov, B.S., *Kinet. Katal.*, 1976, vol. 27, no. 6, p. 1453.
4. Lur'e, B.A., Chernyshev, A.N., and Svetlov, B.S., *Kinet. Katal.*, 1977, vol. 28, no. 4, p. 842.
5. Zhilinskii, V.V., Lokenbakh, A.K., and Lepin', L.K., *Izv. Akad. Nauk Latv. SSR*, 1986, no. 2, p. 151.
6. Zhilinskii, V.V., Lokenbakh, A.K., and Lepin', L.K., *Izv. Akad. Nauk Latv. SSR*, 1988, no. 5, p. 622.
7. Anan'in, V.N., Belyaev, V.V., Romanenkov, V.E., and Trokhimets, A.I., *Vestsi Akad. Nauk BSSR (Khim.)*, 1989, no. 5, p. 17.
8. Lyashko, A.P., Medvinskii, A.A., Savel'ev, G.G., Il'in, A.P., and Yavorovskii, N.A., *Kinet. Katal.*, 1990, vol. 31, no. 4, p. 967.
9. Yakerson, V.I., Dykh, Zh.L., Subbotin, A.N., Gudkov, B.S., Chertkova, S.V., Radin, A.N., Boevskaya, E.A., Tertchnik, E.A., Golosman, E.Z., and Sarmurzina, R.G., *Kinet. Katal.*, 1995, vol. 36, no. 6, p. 918.
10. Tikhov, S.F., Potapova, Yu.V., Sadykov, V.A., and Fenelonov, V.B., *React. Kinet. Catal. Lett.*, 2001, vol. 73, no. 1, p. 55.
11. Tikhov, S.F., Fenelonov, V.B., Zaikovskii, V.I., Potapova, Yu.V., and Sadykov, V.A., *Micropor. Mesopor. Mater.*, 1999, vol. 33, p. 137.
12. Tikhov, S.F., Salanov, A.N., Palesskaya, Yu.V., Sadykov, V.A., Kustova, G.N., Litvak, G.S., Rudina, N.A., Zaikovskii, V.A., and Tsybulya, S.V., *React. Kinet. Catal. Lett.*, 1998, vol. 64, no. 2, p. 301.
13. Tikhov, S.F., Chernykh, G.V., Sadykov, V.A., Salanov, A.N., Alikina, G.M., Tsybulya, S.V., and Lysov, V.F., *Catal. Today*, 1999, vol. 53, p. 639.
14. Gregg, S. and Sing, K., *Adsorption, Surface Area, and Porosity*, New York: Academic, 1982.
15. Rozovskii, A.Ya., Bashkirov, A.N., Kagan, Yu.B., and Pokrovskaya, E.G., *Kinet. Katal.*, 1961, vol. 11, no. 6, p. 830.
16. Rozovskii, A.Ya., *Kinetika topokhimicheskikh reaktsii (The Kinetics of Topochemical Reactions)*, Moscow: Nauka, 1980.
17. Barre, P., *Cinetique Heterogene*, Paris: Gauthier-Villar, 1976.
18. Fenelonov, V.B., *Kinet. Katal.*, 1994, vol. 35, no. 5, p. 795.
19. Krivoruchko, O.P., Zolotovskii, B.P., Plyasova, L.M., Buyanov, R.A., and Zaikovskii, V.I., *React. Kinet. Catal. Lett.*, 1982, vol. 21, p. 103.
20. Buman, R.K., Mironovich, A.A., Chertov, V.M., Tsyryna, V.V., and Tsielen, U.A., *Izv. Akad. Nauk Latv. SSR*, 1988, no. 6, p. 691.
21. Zagrafskaya, R.V., Karnaukhov, A.P., and Fenelonov, V.B., *Kinet. Katal.*, 1976, vol. 17, no. 3, p. 130; 1979, vol. 20, no. 2, p. 465.
22. Fenelonov, V.B., Romannikov, V.N., and Derevyankin, A.Yu., *Micropor. Mesopor. Mater.*, 1999, vol. 28, p. 57.